J. Fluid Mech. (1992), *vol.* 243, *pp.* 133–154
Printed in Great Britain

Internal solitary wave breaking and run-up on a uniform slope

By KARL R. HELFRICH
Woods Hole Oceanographic Institution, Woods Hole, MA 02543, USA

(Received 23 August 1991 and in revised form 18 February 1992)

Laboratory experiments have been conducted to study the shoaling of internal solitary waves of depression in a two-layer system on a uniform slope. The shoaling of a single solitary wave results in wave breaking and the production of multiple turbulent surges, or boluses, which propagate up the slope. Significant vertical mixing occurs everywhere inshore of the breaking location. The kinematics of the breaking and bolus runup are described and a breaking criterion is found. The energetics of the breaking are investigated. Over the range of parameters examined, 15 (± 5) % of the energy lost from first-mode wave motion inshore of the break point goes into vertical mixing.

1. Introduction

The common occurrence of large-amplitude internal waves in coastal regions and straits (Fu & Holt 1982) makes their dynamics of interest. In coastal regions the usual description is of a packet of several first-mode waves propagating on the main pycnocline towards shallower water. There is little evidence of reflection, so all of the incident energy must be dissipated in the shoaling process. The manner in which this dissipation takes place is important since wave instabilities and breaking can lead to vertical mixing and the redistribution of nutrients (Haury, Briscoe & Orr 1978; Sandstrom & Elliott 1984). Sandstrom & Elliott (1984) estimate that if 10% of the incident energy flux goes into vertical mixing, then just several large waves per tidal cycle provide enough mixing to supply all of the required nutrients to the euphotic zone on the Scotian Shelf. Chapman *et al.* (1991) report evidence of run-up of dense water onto the shallow shelf of Palawan Island in the Sulu Sea produced by the breaking of large internal waves. However, details of the wave breaking, both kinematics (i.e. where breaking occurs) and dynamics (i.e. energy conversion to mixing), are not well known.

The usual approach for describing long internal wave evolution in coastal regions has employed Korteweg–de Vries (KdV) theory. The theory assumes a balance between weak nonlinearity and weak dispersion. It is this balance which results in the familiar solitary waves. In a two-layer system the solitary wave is a wave of elevation (depression) for $d_+/d_- > 1$ (< 1), where d_+ and d_- are the depths of the upper and lower layers respectively. KdV theory has compared favourably with observed wave characteristics for both field data (Osborne & Burch 1980; Sandstrom & Elliott 1984) and laboratory experiments (Segur & Hammack 1982; Helfrich & Melville 1986) in cases where the waves are stable. A major limitation of KdV theory is that it does not permit breaking (Whitham 1974) and therefore is of limited value in describing wave instabilities.

Issues of internal solitary wave stability over topography have been addressed in several laboratory experiments. Kao, Pan & Renouard (1985) studied the propagation of internal solitary waves in a two-layer system over slope–shelf topography. The upper layer was always shallower than the lower layer so that solitary waves of depression could exist everywhere. They found that as a solitary wave moved up the slope its rear face steepened. In the vicinity of the shelf break the rear face became unstable and mixing occurred. The instability was attributed to interfacial shear.

Helfrich & Melville (1986, hereafter referred to as HM) also examined the propagation of first-mode solitary waves over slope–shelf topography. In contrast to Kao *et al.* (1985), they considered the situation where the relative layer depths change as the wave moves from a deep region ($d_+ < d_-$) over a uniform slope onto the shelf ($d_+ > d_-$). As the incident wave of depression propagates up the slope it will encounter a point where $d_+ = d_-$ (the turning point), past which it can no longer exist as a wave of depression. Numerical solutions of an extended KdV equation for this 'turning point' geometry show that the incident wave scatters into a packet of oscillatory waves from which one or more solitary waves of elevation emerge (Helfrich, Melville & Miles 1984). In corresponding laboratory experiments HM found that the incident wave could be unstable in the neighbourhood of the shelf break. Instabilities lead to localized vertical mixing.

Cacchione & Southard (1974) and Wallace & Wilkinson (1988) studied the breaking and runup of periodic internal waves in a two-layered system on a uniform slope. Both studies considered the case where the lower layer was always shallower than the upper layer. Therefore, no turning point was encountered. Wallace & Wilkinson (1988, hereafter refered to as WW) found that as the waves shoaled they steepened into an approximately periodic train of solitary waves of elevation. Eventually the rear face of each wave would steepen and overturn. The overturning produced one turbulent vortex, or bolus, of dense water that propagated up the slope until it was eventually dissipated by friction and the continual drainage of mixed fluid back down the slope. They observed that breaking was initiated by the interaction of the incident wave with the return flow from the preceeding wave. WW estimated, but did not measure, that about 3% of the incident energy was converted to a potential energy increase of the water column in the breaking and run-up region.

Cacchione & Wunsch (1974) and Ivey & Nokes (1989) conducted laboratory experiments on the shoaling of periodic internal waves in a continuously stratified fluid on a uniform slope. Wave interaction with the slope produced instabilities and mixing in the bottom boundary layer over the slope. Mixing was most intense when the slope was at the critical angle.

In this paper the results of laboratory experiments on the breaking and run-up of solitary waves of depression in a two-layer system on a uniform slope are discussed. The incident wave in a single solitary wave of depression which must encounter a turning point somewhere on the slope. This is the usual situation in coastal regions and has not been examined in the previous uniform slope experiments. The interaction of topographic scattering of the incident wave, produced by passage through the turning point, and run-up on the uniform slope leads to new results.

The experimental set-up and relevant parameters are described in §2. The results are presented in §3. The kinematics of the breaking and run-up are described. In particular, a breaking criterion is found. Measurements of the energetics show that the wave breaking is efficient in producing vertical mixing. The results are discussed in §4.

2. Experimental set-up and parameters

The experiments were conducted in a glass-walled wave tank 0.65 m deep, 0.40 m wide, and 18 m long (see figure 1). A uniform slope was fabricated using sections of plate-glass which were sealed to the tank walls. A two-layered salt-stratified system was constructed by filling the tank to the desired lower layer depth with salt water of specified density. Prior to adding a layer of fresh water, both the fresh water and the salt water were allowed to sit overnight to allow them to come into thermal equilibrium with the laboratory. The fresh water was then slowly spread over the salt water. This produced a two-layer system with an interfacial thickness of 1.5–2 cm (see figure 16).

Interfacial solitary wave generation and measurement were similar to those described in HM. Interfacial solitary waves were generated using a stepping-motor-driven flap-type wave maker situated in the interface. The flap motion was programmed to give layer mass fluxes that approximate the passage of a single solitary wave. Precision Measurement Engineering micro-scale conductivity-temperature probes (Model 125) were used to measure basic-state density profiles and interfacial displacements. Positioning and profiling of the probes was done with computer-controlled stepping motors. Water samples of known densities (measured with a precision electronic densiometer) were used to calibrate the conductivity probes.

Three probes were used in an experimental run. The first was located at the beginning of the slope (5–7 m from the tip of the wave maker), the second was located inshore of the turning point and the third was positioned at the undisturbed interface–slope intersection, approximately 0.5 cm above the bottom.

Interfacial displacements at the first two probes were calculated assuming lowest-mode motion. Prior to a run, the probes were positioned within the interfacial region. Measured time series of conductivity were converted to equivalent vertical displacements of the static conductivity profiles. This method was used successfully by HM who estimated the error in measured displacements to be less than 10%. The third probe was used to measure the density signal produced by the run-up process.

Side-view photographs and video recordings of shadowgraphs and dye movement were used to obtain quantitative information on the kinematics of breaking and run-up.

For all the experiments, the layer depths before the slope were the same: $d_+ = 10$ cm and $d_- = 26$ cm. Slopes s of 0.034, 0.050 and 0.067, and relative layer density differences

$$\frac{\Delta\rho}{\rho} = \frac{\rho_+ - \rho_-}{\rho_+}$$

of 0.012 and 0.024 were examined. Here ρ_+ (ρ_-) is the density of the upper (lower) layer. Incident solitary waves of amplitudes $a_0 = -0.7$ to -3.4 cm, measured at the beginning of the slope, were studied. Here the amplitude a_0 is the maximum vertical displacement of the interface.

The important independent non-dimensional parameters in addition to $\Delta\rho/\rho$ and d_+/d_- are the nonlinearity parameter

$$\alpha = \frac{a_0}{(d_+ + d_-)}, \tag{1}$$

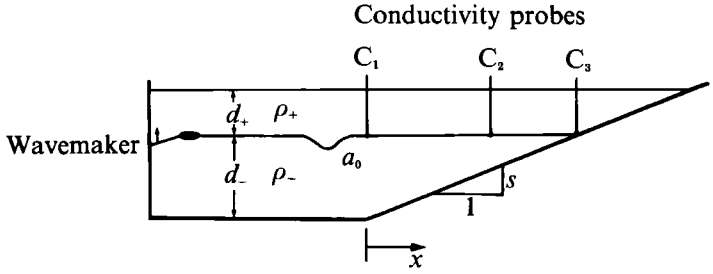

FIGURE 1. Experimental set-up.

based on the wave amplitude and total depth at the beginning of the slope, and the topography parameter

$$\lambda = (kL)^{-1}. \tag{2}$$

Here λ is the ratio of the wave lengthscale k^{-1} to the distance $L = d_- s^{-1}$ from the beginning of the slope to the undisturbed interface–slope intersection. For these experiments k^{-1} is taken from the relation for the wavelength of a KdV solitary wave in a two-layer system (Segur & Hammack 1982),

$$k^{-1} = \left(\frac{4}{3}\frac{d_+^2 d_-^2}{(d_+ - d_-)a_0}\right)^{\frac{1}{2}}. \tag{3}$$

The experiments cover the range $\alpha = [-0.02, -0.093]$ and $\lambda = [0.05, 0.20]$. The incident waves are weakly nonlinear and the slopes are long with respect to the wavelength. Since α and λ are the same order of magnitude, nonlinear and topographic influences are comparable. These scalings are consistent with oceanic observations (HM).

3. Experimental results

Figure 2 shows the interfacial displacements $\eta(t)$, normalized by $-a_0$, at $x/L = 0$ ($x = 0$ is taken to be at the start of the slope) and at $x/L = 0.67$ for an experiment with $\alpha = -0.052$, $\lambda = 0.105$, $s = 0.050$ and $\Delta\rho/\rho = 0.0241$. The second probe is just inshore of the turning point ($x/L = 0.62$). Also shown is the density $\rho(t)$ recorded by the probe positioned at the undisturbed interface–slope intersection. Time has been normalized by c_0/L, where

$$c_0 = \left(g\frac{\Delta\rho}{\rho}\frac{d_+ d_-}{d_+ + d_-}\right)^{\frac{1}{2}} \tag{4}$$

is the linear phase speed at the beginning of the slope and g is the acceleration due to gravity. At $x/L = 0$ (figure 2a) an isolated solitary wave of depression is observed. At $x/L = 0.67$ the leading face of the wave has lengthened and the rear face has steepened. The long, low-amplitude disturbance immediately following the steepened wave between $tc_0/L = 2.6$ and 4.0 is a reflected wave. It appears at the beginning of the slope (figure 2a) between $tc_0/L = 3.5$ and 4.5. The density record at the interface–slope intersection, $x/L = 1.0$, shows that wave shoaling results in a slow decrease in density as the leading face of the incident wave moves up the slope. This corresponds to a down-slope movement of the interface–slope intersection. This is followed by four distinct rises in density and an irregular return to the initial density.

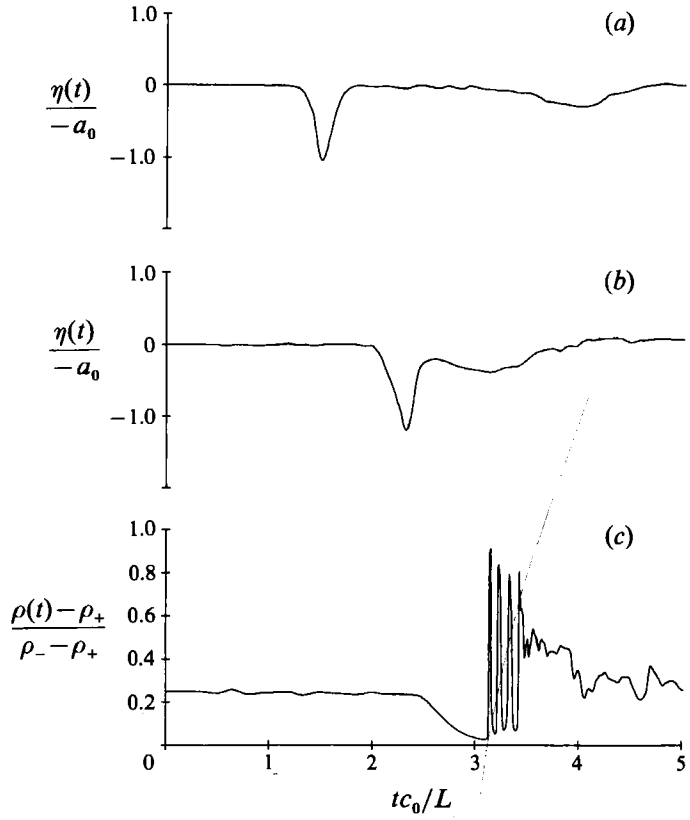

FIGURE 2. Results from an experiment with $(\alpha, \lambda, s, \Delta\rho/\rho) = (-0.052, 0.105, 0.050, 0.0241)$ and $(c_0, L) = (13.1 \text{ cm/s}, 520 \text{ cm})$. (*a*) $\eta(t)$ at the beginning of the slope $x/L = 0$; (*b*) $\eta(t)$ at $x/L = 0.67$; (*c*) $\rho(t)$ at $x/L = 1.0$.

Side-view shadowgraphs from the same experiment are presented in figure 3. In frame (*a*) the elongated leading face of the wave is parallel to the bottom slope, leaving a thin layer of interfacial fluid on the slope. Breaking occurs on the rear face of the incident wave and results in the generation of turbulence and interfacial mixing (frames *b* and *c*). Several discrete turbulent surges, or boluses, propagate up the slope past the interface–slope intersection (frames *c*–*g*). At the undisturbed interface–slope intersection the boluses contain lower-layer water which has been slightly diluted by mixing (see figure 2*c*). Interfacial mixing occurs everywhere shoreward of the breaking location and is enhanced by the run-up of the boluses, which continue to entrain upper-layer water as they move up the slope.

A second-mode interfacial solitary wave (Davis & Acrivos 1967; Benjamin 1967) is occasionally generated by the breaking and is observed to propagate offshore. These waves are characterized by isolated varicose perturbations of the pycnocline. An example of such a wave is noted by the arrows in frames (*f*) and (*g*). These waves decayed rapidly and were never observed to propagate back to the beginning of the slope. No systematic attempt was made to identify them in individual runs.

Figure 4 shows another example of wave breaking and run-up for a larger incident wave, $\alpha = -0.094$. Both s and $\Delta\rho/\rho$ are the same as in figure 3. The breaking and run-up are similar to the observations for the smaller wave; however, the breaking location has moved further offshore and the mixing is more intense. The boluses are

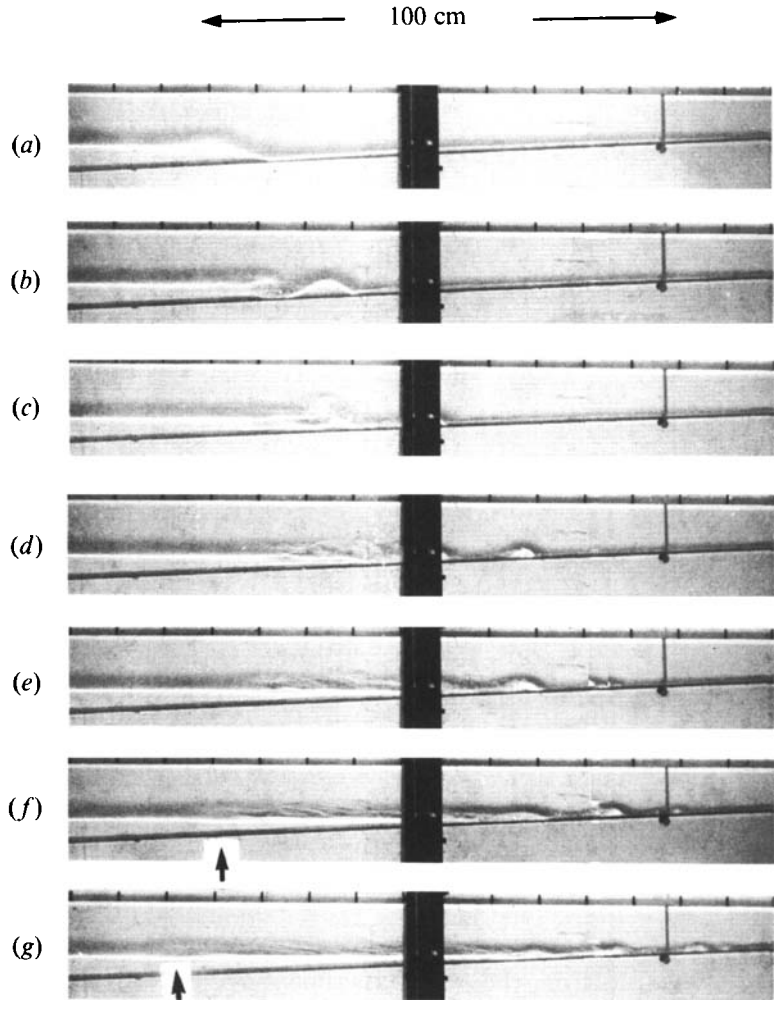

FIGURE 3. Shadowgraphs of wave breaking and runup for the run in figure 2. The thin, dark vertical stripe on the right is the conductivity probe at the interface–slope intersection. (*a*) $tc_0/L = 2.64$, (*b*) 2.74, (*c*) 2.84, (*d*) 2.94, (*e*) 3.04, (*f*) 3.14, (*g*) 3.24. The times correspond to those in figure 2. The arrows in (*f*) and (*g*) indicate the location of a second-mode wave.

larger and propagate further up the slope before they are dissipated. As the slope decreases the strong overturning is not as dominant, although significant interfacial mixing does occur. The initial breaking occurs further offshore as the slope decreases, so that the mixing takes place over a larger extent than for a wave of the same amplitude on a steeper slope.

Photographs of mixing and transport of dye due to breaking and run-up are shown in figure 5 for a run with $(\alpha, \lambda, s, \Delta\rho/\rho) = (-0.075,\ 0.118,\ 0.067,\ 0.0245)$. The horizontal stripe of dye marks the pycnocline and a patch of dye was introduced in the lower layer about 90 cm before the interface–slope intersection. Dye was also placed on the bottom at the positions indicated by the arrows in frame (*a*). As the incident wave shoals it sweeps the dye in the lower layer offshore and out of view (frame *b*). As the wave breaks the dye on the bottom is quickly mixed throughout the lower layer (frames *b* and *c*). Interfacial and upper-layer water is mixed down into the

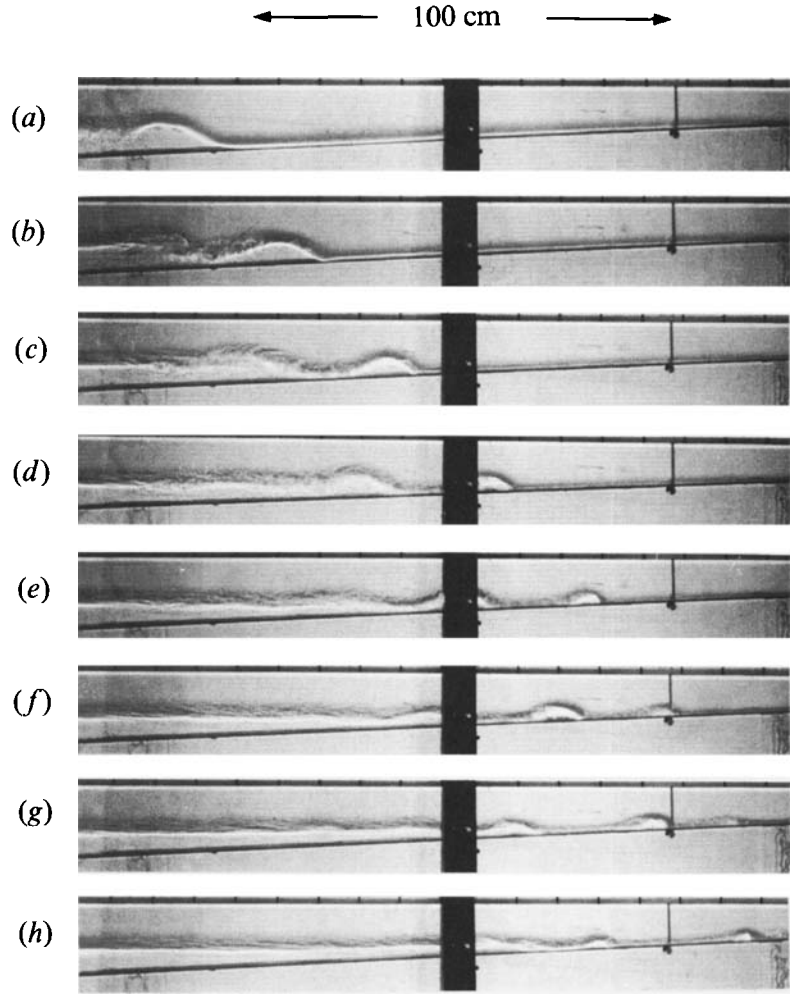

FIGURE 4. Shadowgraphs for a run with a larger incident wave. $(\alpha, \lambda, s, \Delta\rho/\rho) = (-0.094, 0.078, 0.050, 0.0241)$. The time between frames is 4 s.

lower layer. The boluses transport this mixed fluid up the slope (frames *d–i*). Frame (*j*) shows the dye distribution after the surge activity has ceased. Mixed fluid is moving offshore as an intrusive layer in the lower part of the original pycnocline. The patch of dye that was swept offshore has returned to a position slightly inshore of its original location indicating a net onshore flux of lower layer fluid as a result of the breaking and run-up.

3.1. *Kinematics*

The breaking is qualitatively similar to the breaking observed in HM for waves incident on a slope–shelf geometry. The strong down-slope flow in the lower layer, caused by the advancing front face of the incident wave, and up-slope flow immediately behind the rear face, leads to a large horizontal velocity convergence in the lower layer underneath the steepened rear face. Thus, lower-layer vertical velocities are large in this region. Furthermore, the strong flows increase the interfacial shear. HM measured lower-layer particle velocities of the same order as the wave phase speed in the breaking region. Although systematic velocity

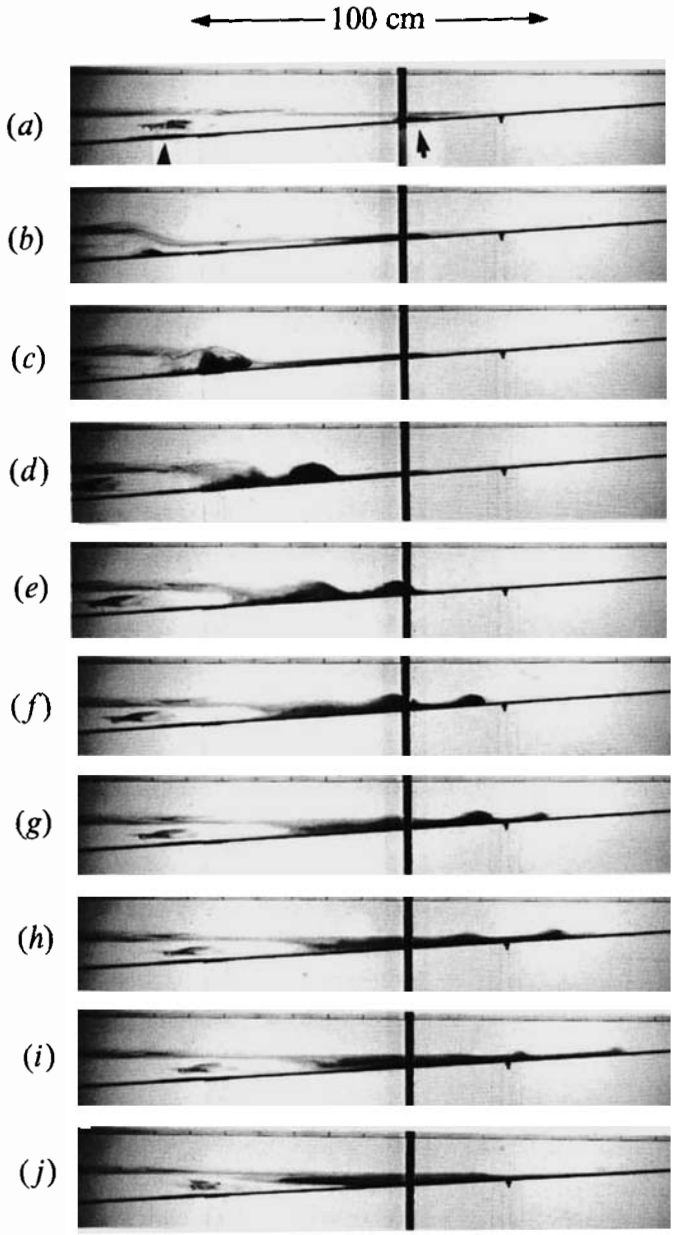

FIGURE 5. Mixing and up-slope transport of dye for a run with $(\alpha, \lambda, s, \Delta\rho/\rho) = (-0.075, 0.118, 0.067, 0.0245)$. Frame (a) was taken before wave generation. The time between frames from (b) to (i) is 4 s. Frame (j) was taken 26 s after frame (i).

measurements were not undertaken in the present experiments, observations of neutral-density particles showed that lower-layer velocities were comparable with the local wave phase speed during the breaking events.

The location of the wave instability, or break point, was defined as the maximum offshore location of the initial patch of turbulence. The shadowgraph images were used to identify this location. From these observations a breaking criterion was determined and is shown in figure 6 where $-a_0/d_{-\mathrm{BP}}$ is plotted against λ. Here $d_{-\mathrm{BP}}$

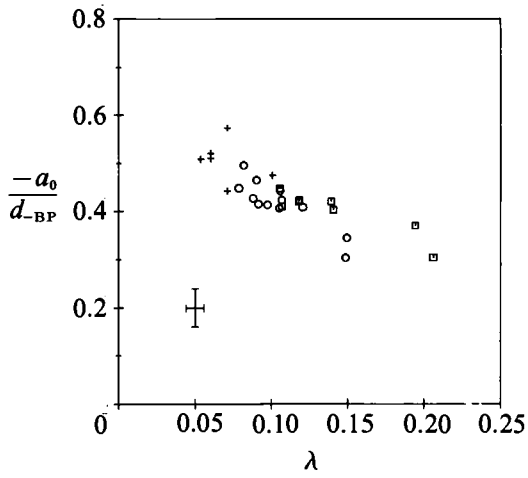

FIGURE 6. Breaking location (criterion): +, $s = 0.034$; ○, 0.050; ⊡, 0.067. The error bars represent the uncertainty in the measurements.

is the undisturbed lower-layer depth at the break point and a_0 is the wave amplitude measured at the beginning of the slope (probe C_1 in figure 1). Over the range of parameters examined, breaking occurs where the undisturbed lower-layer depth is about 2–3 times a_0. There is a tendency for $-a_0/d_{-BP}$ to increase as λ decreases. Decreasing λ corresponds to decreasing the slope (increasing L) or increasing the incident wave amplitude, since k^{-1} decreases as $-a_0$ increases (see (3)). Larger waves tend to propagate into slightly shallower water (relative to their initial amplitude) before breaking than do smaller waves.

Figure 6 includes data from experiments with $\Delta\rho/\rho = 0.012$ and 0.024. There was no systematic difference due to $\Delta\rho/\rho$ in this and other observations, except for wave and bolus propagation speeds. However, the propagation speed differences could be scaled by the density difference. Henceforth, all the data will be grouped together and differences in $\Delta\rho/\rho$ will not be noted.

The breaking criterion in figure 6 is similar to the one found in HM for internal solitary waves incident on slope–shelf topography. They found that for

$$-a_0/d_{-S} \lesssim 0.3,$$

where d_{-S} is the depth of the lower layer on the shelf, the incident wave would move on to the shelf with no instabilities. For $-a_0/d_{-S} \gtrsim 0.4$, strong overturning and second-mode wave generation occurred in the neighbourhood of the shelf break. For $0.3 < -a_0/d_{-S} < 0.4$ weaker interfacial shear instabilities were observed. Their results were not dependent upon λ for $\lambda = 0.1$–0.3. The new results for a uniform slope are consistent with these results, suggesting that the mechanism is similar.

The maximum run-up of mixed fluid past the undisturbed interface–slope intersection X_R is plotted against $-a_0$ in figure 7. The runup is approximately a linear function of incident amplitude and independent of the bottom slope. The best fit to the data, $X_R = 1.14$–$18.9a_0$, where a_0 and X_R are given in cm, is also shown. The total distance of mixing and bolus activity X_T can be defined as

$$X_T = X_{BP} + X_R, \tag{5}$$

where

$$X_{BP} = d_{-BP}/s \tag{6}$$

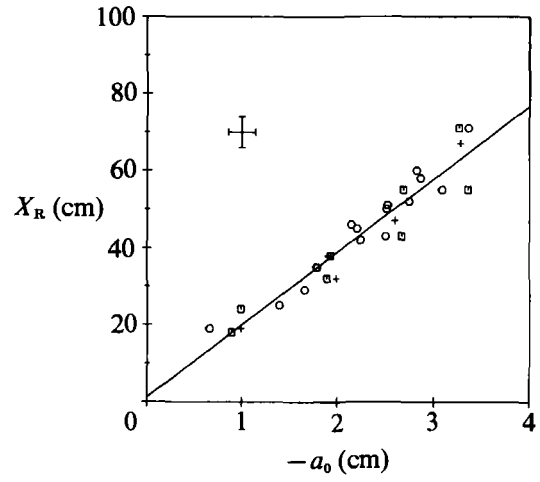

FIGURE 7. Maximum runup past the undisturbed interface–slope intersection: +, $s = 0.034$; ○, 0.050; ⊡, 0.067.

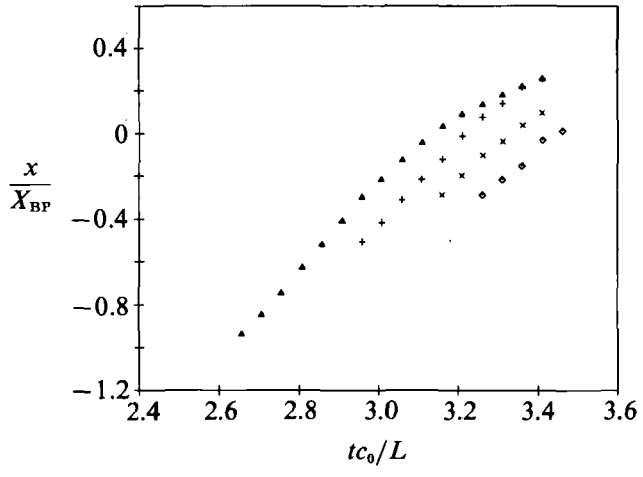

FIGURE 8. Location of boluses in (x, t) space for the run shown in figures 2 and 3. Each symbol corresponds to one bolus.

is the distance from the break point to the undisturbed interface–slope intersection. Taking $-a_0/d_{-BP} = 0.4 \pm 0.1$ from figure 6 and $X_R/(-a_0) = 19 \pm 1$ from figure 7, we get

$$X_T/-a_0 \approx 2.5s^{-1} + 19. \tag{7}$$

Since $2.5s^{-1} > 19$, most of the bolus runup, and therefore vertical mixing, occurs offshore of the undisturbed interface–slope intersection.

Figure 8 shows an x–t diagram of bolus locations for the experimental run in figures 2 and 3. The times correspond to those in figures 2 and 3, and the distance x (positive onshore) from the undisturbed interface–slope intersection has been normalized by X_{BP}. Points are plotted only when the boluses are clearly identifiable. The figure shows several features which are typical of all the experiments. The lead bolus is formed first and furthest offshore. Subsequent boluses form later and progressively up the slope. The number of boluses present at any one time is not constant. New boluses are formed as older ones dissipate. However, all appear before the

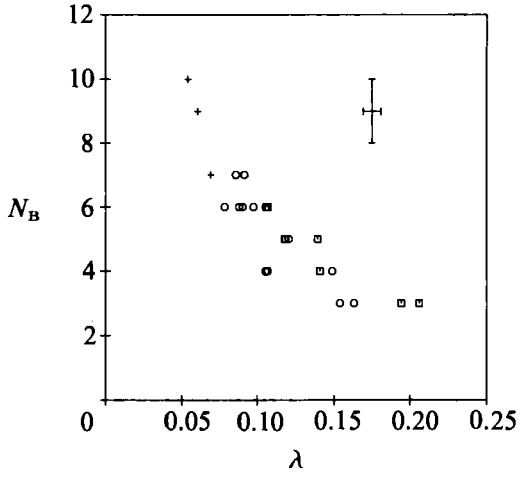

FIGURE 9. Number of boluses produced in a breaking event: +, $s = 0.034$; ○, 0.050; ⊡, 0.067.

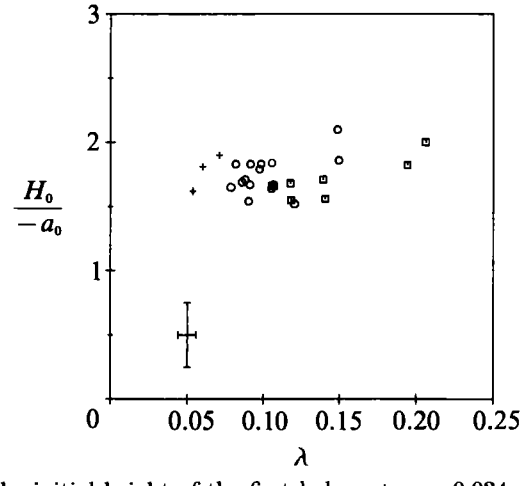

FIGURE 10. The initial height of the first bolus: +, $s = 0.034$; ○, 0.050; ⊡, 0.067.

undisturbed interface–slope intersection and dissipate after passing through this location. The first bolus is often overtaken and absorbed by the second bolus, which may in turn be overtaken; though this did not occur in this particular run. For all the runs, the initial speed of a bolus $c_{B0} \approx 0.6 c_{0BP}$, where c_{0BP} is the linear phase speed at the break point (i.e. $d_- = d_{-BP}$ in (4)).

Since all the boluses pass the undisturbed interface–slope intersection, the total number of boluses produced by the breaking of a single incident wave, N_B, was determined from the density recorded at this point. For example, the run in figure 2(*c*) shows the passage of four distinct surges, which is consistent with figure 8. In other runs, identification of boluses is not always as clear, so the determination of N_B has an uncertainty of one. Figure 9 shows N_B plotted against λ. The data show that N_B increases rapidly as λ decreases. Either increasing $-a_0$, or decreasing the slope will result in an increase in the number of surges.

The initial height of the first bolus formed after breaking, H_0 is shown in figure 10 where $H_0/(-a_0)$ versus λ is plotted. Here H_0 is defined as the height of mixed fluid comprising the bolus and is measured immediately after the bolus is clear of the

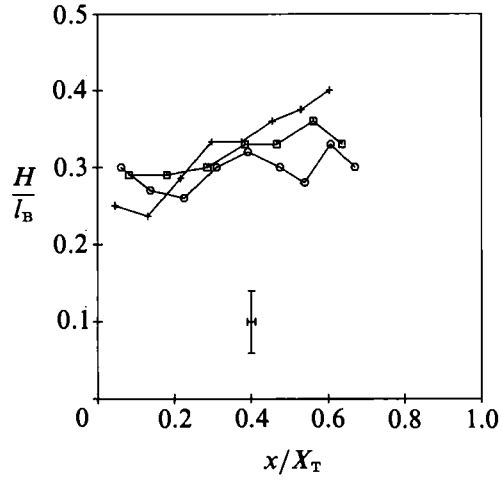

FIGURE 11. First bolus aspect ratio H/l_B versus up-slope distance for runs with $\alpha \approx -0.053$: +, $s = 0.034$; ○, 0.050; ⊡, 0.067.

breaking region. The data show $H_0/(-a_0) = 1.75 \pm 0.25$, with no clear dependence upon λ. In all cases the first bolus was the largest. Subsequent boluses decreased in amplitude.

The characteristics of the boluses observed here are similar to those described by WW for boluses produced by a train of internal solitary waves of elevation shoaling on a uniform slope (no turning point encountered on the slope). They found that each bolus had a self-preserving shape with an aspect ratio $H/l_B \approx 0.3$, independent of bottom slope and incident energy flux. Here H is the height of the mixed core of the bolus and l_B is the length measured at the bottom of the bolus core. They derived a simple analytical model in which the change in bolus momentum was balanced by down-slope buoyancy and bottom friction. Their model gives

$$\frac{H}{H_0} = 1 - \frac{x}{x_0} \tag{8}$$

and

$$\frac{c_B}{c_{B0}} = \left(1 - \frac{x}{x_0}\right)^{\phi}. \tag{9}$$

Here x is measured from the point of bolus formation, x_0 is the total runup distance (equal to X_T given by (5)), c_B is the bolus propagation speed, c_{B0} is the initial speed, and ϕ is a constant which depends upon a drag coefficient and other parameters (see equation (11) in WW).

In figure 11 the aspect ratio H/l_B of the first bolus produced during a breaking event is plotted against x/X_T, for an incident wave amplitude $a_0 = -1.9$ cm ($\alpha = -0.053$). Data were obtained from analysis of shadowgraphs. H and l_B are defined as above. For all slopes $H/l_B \approx 0.3$, although for $s = 0.034$ there is a tendency for H/l_B to increase with x. This increase may be related to the reduction in the intensity of breaking (overturning and mixing) which occurs as the slope decreases. Data for the other incident wave amplitudes also give $H/l_B = 0.3 \pm 0.1$. Second, and subsequent boluses also have $H/l_B \approx 0.3$. However, measurements of the characteristics of these trailing surges have more uncertainty since the trailing surges are interacting with the wake of the preceeding boluses.

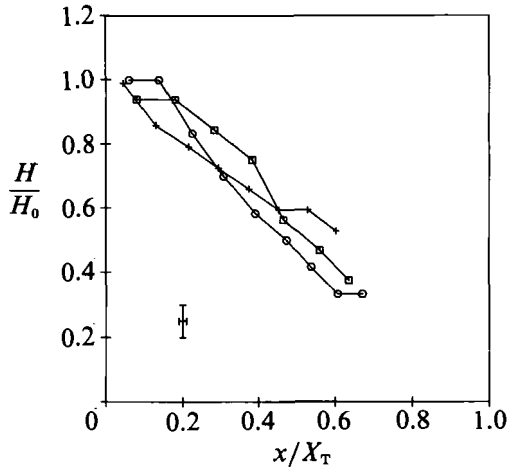

FIGURE 12. Decay of the first bolus height with distance for the runs in figure 11.

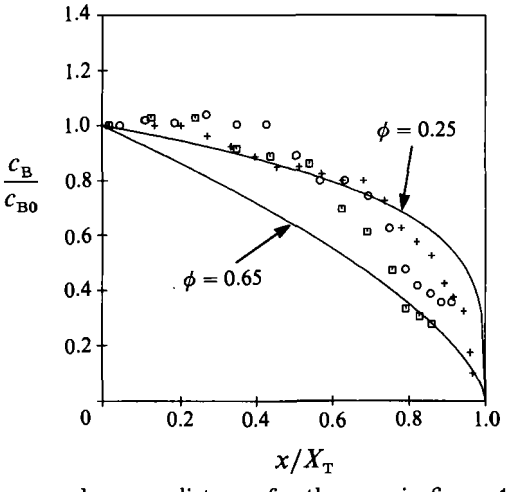

FIGURE 13. First bolus speed versus distance for the runs in figure 11. The solid lines correspond to (9) with $\phi = 0.25$ and 0.65.

Figure 12 shows the decay of the first bolus height with distance for the runs with $\alpha = -0.053$. H/H_0 decreases approximately linearly as predicted by (8). Figure 13 shows c_B/c_{B0} versus x/X_T for the same runs as figure 12. Also shown is the model prediction (9) for $\phi = 0.25$ and 0.65. The value of $\phi = 0.65$ lies in the range 0.6–0.7 that WW found gave the best fit to their data for run-up on slopes of 0.030 and 0.054. The value of $\phi = 0.25$ gives a prediction which is closer to the present experimental data. Both the linear decrease in bolus height and the slow initial decrease in bolus speed are found for all the incident wave amplitudes.

The difference in ϕ may be due to the effect of the upper layer on bolus evolution. In WW's experiments the upper layer was deep ($d_+ = 37.5$ cm at the interface–slope intersection) so that bolus heights were very small relative to the upper-layer depth. Forced horizontal velocities in this layer would therefore be small. In the present experiments the upper layer was shallow and bolus heights were a significant fraction of the total water depth in the run-up region. Boluses should interact strongly with the upper layer as they run up the slope. Furthermore, a solitary wave of depression has upper-layer velocities of order $c_0 a_0/d_+$ directed onshore. This wave-induced

upper-layer flow may affect the bolus runup, possibly by helping to advect them onshore. Upper-layer motion, accounted for in WW's equation for ϕ by an added-mass coefficient, may be more important in the present experiments. Indeed, increasing the added-mass coefficient in WW's theory causes ϕ to decrease, consistent with these experiments. Also note from figure 13 that the first bolus speed does not decrease very much until $x/X_T = 0.6$–0.7. From (6) and (7)

$$\frac{X_{BP}}{X_T} \approx \frac{2.5s^{-1}}{2.5s^{-1}+19} = 0.7\text{–}0.8$$

for $s = 0.067$–0.034. The rapid decrease in bolus speed begins just before the bolus reaches the location of the undisturbed interface–slope intersection.

3.2. *Energetics*

Wave energy incident on the slope will be dissipated in either viscous boundary layers (bottom, sidewall and interfacial) or in breaking events, and some energy will be reflected. A fraction of the energy lost to breaking will go into vertical mixing, resulting in a net increase in the potential energy of the water column. This redistribution of wave energy can be examined from the experimental data. Of particular interest is the mixing efficiency of the wave breaking. The mixing efficiency, Σ, is given by

$$\Sigma = \frac{\Delta P_{BP}}{E_N}, \tag{10}$$

where ΔP_{BP} is the change in potential energy inshore of the break point and

$$E_N = E_{BP} - E_R \tag{11}$$

is the net energy into the breaking region. The net energy is composed of the onshore energy at the break point E_{BP} and the reflected energy E_R. The breaking region is defined to be everywhere inshore of the break point.

The wave energy E per unit width through, or work on, a vertical section between times t_1, and t_2 is given by

$$E = \int_{t_1}^{t_2} \int_{-h}^{0} [p(z)\,u(z) + \bar{\rho}(z)\,u(z)^3]\,\mathrm{d}z\,\mathrm{d}t, \tag{12}$$

where $p(z)$ and $u(z)$ are the wave-induced pressure and horizontal velocity respectively. Here $\bar{\rho}(z)$ is the background vertical density profile, h is the water depth and z is the vertical coordinate, equal to zero at the free surface. For long, weakly nonlinear waves (i.e. KdV approximation) in a two-layer system (12) becomes

$$E = c_0 g(\rho_+ - \rho_-) \int_{t_1}^{t_2} \eta(t)^2\,\mathrm{d}t + O(\alpha). \tag{13}$$

Here $\eta(t)$ is the interfacial displacement at the location where E is to be evaluated. Over the slope where the lower-layer depth is changing, d_- and c_0 are the local values of lower-layer depth and linear phase speed, respectively. The approximation leading to (13) is appropriate for these experiments and the errors introduced are within the experimental uncertainty. In calculating energy with (13) we are neglecting energy of second- or higher-mode waves. Although some second-mode waves were observed, their contribution to the energy budget is insignificant.

The incident energy E_0 is evaluated with $\eta(t)$ measured at the beginning of the slope ($x/L = 0$). The times t_1 and t_2 are chosen so that just the incident solitary wave is included in the evaluation of (13).

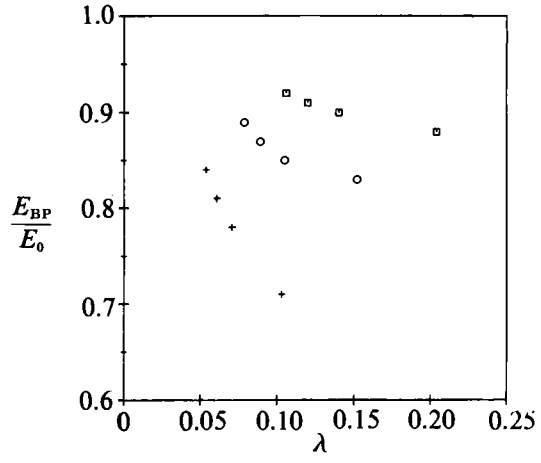

FIGURE 14. Theoretically computed fraction of incident energy at the break point: +, $s = 0.034$; ○, 0.050; ⊡, 0.067.

To evaluate E_{BP} the fraction of incident wave energy lost to viscous dissipation between the beginning of the slope and the break point must be estimated. E_{BP} is difficult to evaluate directly with the available data (i.e. from the second probe on the slope) because the incident and reflected waves are not clearly separated (i.e. the specification of t_2 is not obvious). For example, figure 2(*b*) shows that the incident and reflected waves are not completely separated at $x/L = 0.67$. As an example, we take $t_2 c_0/L = 2.57$ in figure 2(*b*) then $E/E_0 \approx 0.90$, and about 10% of the incident energy is lost to viscous processes up to this point. However, the uncertainty is large and, as the slope or incident amplitude increases, the separation of the incident and reflected waves in the interfacial displacement record on the slope becomes even less well defined.

HM showed that, in the absence of breaking, the KdV model including viscous boundary-layer dissipation gives good prediction of wave evolution and dissipation over slope–shelf topography. Wave dissipation due to viscous process was calculated to within 5% for evolution distances much longer than those considered here. Thus for evolution up to breaking the model can be used to estimate dissipation in the present problem. The model details and scaling requirements are given in Appendix A. The results were obtained for the experimental parameters $(d_+, d_-, \Delta\rho/\rho) =$ (10 cm, 26 cm, 0.024), $s = 0.034$, 0.050 and 0.067, and a kinematic viscosity of 0.01 cm^2 s^{-1}. The initial conditions were solitary waves with amplitudes $a_0 = -0.9$, -1.9, -2.6 and -3.3 cm at the beginning of the slope. The model was integrated up to the break point given by figure 6 for each value of λ.

Figure 14 shows the results of numerical calculations of the onshore energy transport at the break point E_{BP}, normalized by E_0. Between 10 and 30% of the incident energy is dissipated on the slope prior to breaking. The fraction of energy dissipated increases as either s or $-a_0$ decreases. For the conditions of figure 2, $\lambda = 0.105$ and $s = 0.050$, the model predicts $E_{BP}/E_0 = 0.85$. At $x/L = 0.67$ the model predicts $E/E_0 = 0.91$. This compares favourably with the value of 0.9 estimated above for the data in figure 2 at $x/L = 0.67$.

It was possible to evaluate the energy content of the reflected wave E_R measured at the beginning of the slope. This was done by choosing t_1 and t_2 so that only the reflected wave, always well separated from the incident wave, was included in the evaluation of (13). For example, in figure 2(*a*), t_1 and t_2 were chosen to be

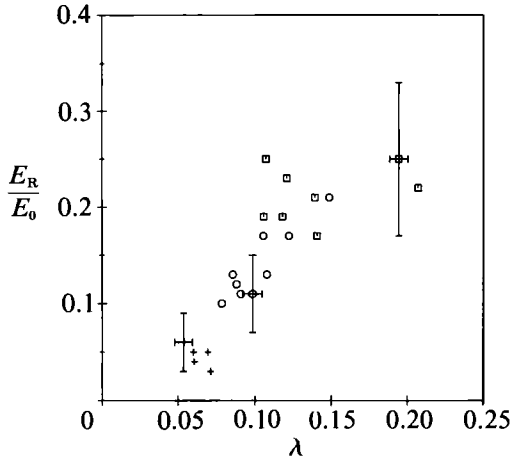

FIGURE 15. Reflected energy: +, $s = 0.034$; ○, 0.050; ⊡, 0.067.

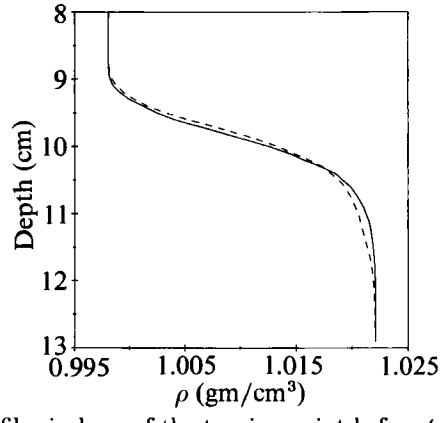

FIGURE 16. Density profiles inshore of the turning point before (——) and after (– – –) a run. $(\alpha, \lambda, s, \Delta\rho/\rho) = (-0.094, 0.078, 0.050, 0.0241)$.

$t_1 c_0/L = 3.25$ and $t_2 c_0/L = 4.50$. Figure 15, where E_R/E_0 versus λ is plotted, shows the results. There is an uncertainty in E_R/E_0 of $\pm 30\%$, determined by varying t_1 and t_2 for a given run. The fraction of incident energy reflected increases as λ increases (i.e. smaller wave amplitudes or steeper slopes) and reaches 0.2–0.25 for $\lambda = 0.15$–0.2. The smallest slope ($s = 0.034$) reflected only about 5% of the incident energy.

Mixing produced by breaking and bolus runup lead to measurable changes in the potential energy of the system. Wave-induced mixing produced a thickened pycnocline inshore of the break point. It would then move offshore as an intrusion. To prevent the intrusion from spreading the length of the tank, where its effect on the background density profile would be undetectable, a vertical gate was inserted at the turning point after passage of the incident and reflected waves, but before the arrival of the mixed fluid. After all motion had ceased (≈ 15 minutes), several density profiles inshore and offshore of the gate were obtained. The time that the gate was in place was short enough so that the buoyancy flux driven by diffusive processes in the region where the pycnocline intersects the slope (Phillips 1970) was negligible. Profiles taken offshore of the gate showed no measurable differences from before and after a run. Differences in density profiles inshore of the gate were attributed entirely to wave breaking. Figure 16 shows a typical pair of density profiles from before and after a run.

Changes in potential energy (per unit width) in the region inshore of the turning point, ΔP_{TP}, were found from

$$\Delta P_{TP} = \int_{-h}^{0} g\Delta\rho(z)\, B(z)\, z\mathrm{d}z, \tag{14}$$

where

$$\Delta\rho(z) = \rho_f(z) - \rho_i(z) \tag{15}$$

is the difference between the initial profile ρ_i and the profile taken after breaking ρ_f. Here

$$B(z) = \frac{h}{s}\left(1 + \frac{z}{h}\right) \tag{16}$$

is the horizontal extent of the triangular region at a depth z. Here $z = 0$ is the free surface and $h = 2d_+$ is the total depth at the turning point.

The turning point was chosen for the gate location because it is a convenient division between onshore and offshore. However, to evaluate Σ from (10) the change of the potential energy inshore of the break poing ΔP_{BP} must be determined. Some potential energy is lost to kinetic energy, and ultimately viscous dissipation, as the mixed fluid spreads offshore from the breaking region to the gate. The potential energy change that would arise if all the mixed fluid had been confined to inshore of the break point is shown in Appendix B to be

$$\Delta P_{BP} = \Delta P_{TP} X_{TP}/X_{BP}, \tag{17}$$

where $X_{TP} = d_+ s^{-1}$ is the distance from the turning point to the interface–slope intersection and ΔP_{TP} is given by (14). There is an additional correction due to the sloping bottom, but it is small.

The mixing efficiency (10) could then be evaluated. ΔP_{BP} from each run was calculated from (17) using measurements of ΔP_{TP} with X_{BP} found from figure 6. The net energy (11) was determined as follows. The energy E_{BP} was found using figure 14 given measurements of E_0 and the appropriate values of λ and s. The energy reflected from the breaking region was set equal to the reflected energy measured at the beginning of the slope (figure 15). There is some dissipation of the reflected energy between the break point and the beginning of the slope. Corrections due to this effect, using figure 14, change estimates of Σ by about 3% which is well within the uncertainty of the rest of the data. Measurements of ΔP_{BP} are accurate to $\pm 25\%$ based upon variations in ΔP_{BP} from the several density profiles taken after each run. Incident energy E_0 measurements are accurate to $\pm 10\%$. Estimates of dissipation of incident energy on the slope are good to $\pm 5\%$ and the reflected energy E_R is estimated to $\pm 30\%$. These possible errors result in a maximum uncertainty for each calculated value of Σ of $\pm 50\%$.

Figure 17 shows the mixing efficiency for all the runs in which potential energy changes were measured. The average value for all the data points is $\Sigma = 0.15$. The scatter of the data (± 0.05) is consistent with the estimated uncertainty. Dependence of Σ on λ or other parameters cannot be discerned. The average value $\Sigma = 0.15 \pm 0.05$ is the principal result.

3.3. *Multiple incident waves*

Finally we note that in the coastal regions the large internal waves incident on the slopes typically occur as groups of nonlinear waves rather than isolated solitary waves. To examine the effect of multiple waves several experiments were run with two solitary waves of the same amplitude, separated by several wavelength scales, incident on the slope $s = 0.067$. Figure 18 shows the measured displacements and

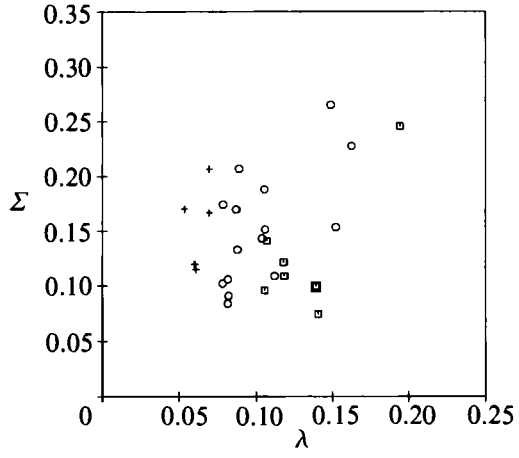

FIGURE 17. The mixing efficiency of wave breaking inshore of the break point: +, $s = 0.034$; ○, 0.050; ⊡, 0.067.

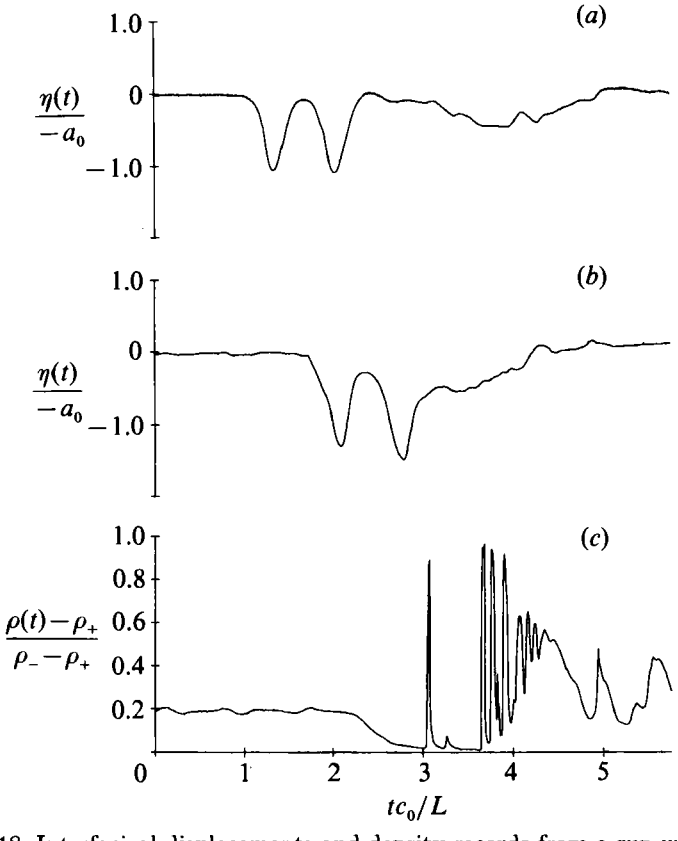

FIGURE 18. Interfacical displacements and density records from a run with two incident solitary waves. $(\alpha, \lambda, s, \Delta\rho/\rho) = (-0.054, 0.139, 0.067, 0.0242)$ and $(c_0, L) = (13.1$ cm/s, 388 cm). (*a*) $\eta(t)$ at $x/L = 0$; (*b*) $\eta(t)$ at $x/L = 0.65$; (*c*) $\rho(t)$ at $x/L = 1.0$.

density at the interface–slope intersection as functions of time for a run with $(\alpha, \lambda, s, \Delta\rho/\rho) = (-0.054, 0.139, 0.067, 0.0242)$. Breaking occurs at the same location as the single wave. Interaction of the waves significantly changes the number and separation of the boluses from what might be anticipated based on superposition of two isolated waves. Measurements of energetics of the breaking for several multiple-wave runs giving mixing efficiencies within the range found for single-wave runs.

4. Discussion

The experiments show that an internal solitary wave of depression incident on a uniform slope will break and produce multiple boluses of primarily lower-layer water which propagate up the slope past the undisturbed interface–slope intersection. A breaking criterion was found and the kinematics of the breaking and bolus runup were described. The characteristics of individual boluses are similar to those described by WW; however, the production of multiple boluses per single incident wave occurs only for the case of solitary waves of depression (i.e. a turning point is present on the slope).

The production of multiple boluses per incident wave can be understood as the result of topographic scattering of the incident wave and subsequent interaction with the slope. A solitary wave of depression in a two-layered system incident on slope–shelf topography with a turning point will scatter into a packet of oscillatory waves on the shelf from which one or more solitary waves of reversed polarity may asymptotically separate from the packet (Djordjevic & Redekopp 1978; Knickerbocker & Newell 1980; Helfrich *et al.* 1984). In these experiments with a slope that intersects the interface, the scattering process is interrupted and the scattered waves are forced to propagate up the slope. The experiments showed that breaking and vertical mixing always occur, leading to the formation of boluses with cores of mixed fluid, particularly for the first few boluses which are largest and most intense. The multiple boluses that emerge on the slope correspond qualitatively to the wave crests that would form the scattered packet. Even in the absence of breaking and mixing the runup of multiple scattered waves, or laminar surges, is expected. It was shown that the number of boluses generated increases as λ is decreased (see figure 9). The numerical studies of solitary waves with slope–shelf geometry showed that the number of solitary waves which emerge on the shelf increases as λ decreases (Helfrich *et al.* 1984). It should be emphasized that the boluses are not positive solitary waves, just that the behaviour is similar, indicating the role of topographic scattering in the production of multiple boluses.

WW observed that wave overturning and breaking did not occur for the first wave incident on the slope. Breaking was initiated by the interaction of an incident wave with the backflow produced by the shoaling of the preceding solitary wave. A single incident solitary wave of elevation may not overturn and break, but simply surge up the slope with little mixing. In the present experiments, all incident waves experienced at least interfacial shearing instabilities, and usually strong overturning. The backflow that WW found was necessary to produce significant mixing may be provided in this case by the rapid offshore flow of lower-layer water that occurs as the front face of the incident wave moves up the slope.

The mixing efficiency inshore of the break-point of 0.15 ± 0.05 is several times larger than the value of 0.03 that WW estimated (but did not measure) for the breaking of a solitary wave of elevation. The increase is certainly due to the generation of multiple boluses which enhance the mixing and onshore transport of

dense water. The efficiencies found here are comparable with the values approaching 0.20 that Ivey & Nokes (1989) measured for monochromatic internal waves in a continuously stratified fluid breaking on a slope at the critical angle. Ivey & Imberger (1991) used existing experimental data to show that turbulence in a stably stratified fluid has flux Richardson numbers, or mixing efficiencies, of 0.20 or less. Scaling of the results on dissipative and turbulent mixing processes up to oceanic scales is difficult because of the large difference in turbulent Reynolds number between the laboratory and the oceanic conditions. Even with this large difference in scales the results suggest that the breaking and runup of internal solitary waves of depression will be an efficient mechanism for mixing in coastal regions.

Cacchione & Southard (1974) have shown that shoaling internal waves are capable of suspending and transporting sediment. The breaking and runup of long, nonlinear internal waves may be a very effective mechanism for onslope sediment transport. The turbulent boluses, which were shown to have phase speeds comparable to the linear phase speed, could suspend and transport sediment up the slope where the larger particles would be deposited as the boluses decay. Fine particles may stay in suspension and be advected offshore with the mixed fluid. The production of multiple boluses per incident wave would enhance this process.

This work was supported by a grant from the National Science Foundation (OCE-8902671). Robert E. Frazel assisted with the photography.

Appendix A

The KdV equation including cubic nonlinearity, variable topography and viscous boundary-layer dissipation has been shown by HM to give good agreement for wave evolution over slope–shelf topography. It is used here to estimate wave dissipation on a uniform slope up to the break point. For a two-layer system the extended KdV equation is, in dimensional form (HM),

$$\Lambda\eta+\frac{\partial\eta}{\partial x}+\alpha_1\eta\frac{\partial\eta}{\partial\theta}+\alpha_2\eta^2\frac{\partial\eta}{\partial\theta}+\beta_1\frac{\partial^3\eta}{\partial\theta^3}=\delta_1\int_{-\infty}^{\infty}\frac{\partial\eta}{\partial\theta'}\frac{1-\mathrm{sgn}\,(\theta-\theta')}{|\theta-\theta'|^{\frac{1}{2}}}\,\mathrm{d}\theta', \tag{A 1}$$

where

$$\Lambda=\frac{1}{2c_0}\frac{\mathrm{d}c_0}{\mathrm{d}x}, \tag{A 2}$$

$$\alpha_1=\frac{3}{2c_0}\frac{d_+-d_-}{d_+d_-}, \tag{A 3}$$

$$\alpha_2=\frac{3}{c_0(d_+-d_-)}\frac{d_+^3+d_-^3}{d_+d_-}, \tag{A 4}$$

$$\beta_1=\frac{d_+d_-}{6c_0^3}, \tag{A 5}$$

and

$$\delta_1=\frac{\nu^{\frac{1}{2}}}{4\pi^{\frac{1}{2}}c_0}\frac{d_+-d_-}{d_++d_-}\left[\frac{2}{wd_+}+\left(1+\frac{2d_-}{w}\right)\frac{1}{d_-^2}+\frac{1}{2}\left(\frac{d_++d_-}{d_+d_-}\right)^2\right]. \tag{A 6}$$

The horizontal coordinate in the inshore direction is x, η is the interfacial displacement, the phase variable

$$\theta=\int_0^x\frac{\mathrm{d}x}{c_0}-t,$$

and t is time. Here c_0 is the linear phase speed given by (4), d_+ is the upper-layer depth, $d_-(x)$ is the variable lower-layer depth, ν is the kinematic viscosity and w is the width of the tank.

The KdV equation (A 1) is valid for long, weakly nonlinear waves over slowing varying topography. Furthermore, it requires the boundary-layer thickness to be much less than the water depth,

$$\frac{1}{d_+ + d_-}\left(\frac{\nu}{c_0 k}\right)^{\frac{1}{2}} \ll 1.$$

The dissipation is weak and is confined to thin laminar boundary layers. A boundary-layer Reynolds number based on the particle velocities ($\approx \alpha c_0$) is $O(10)$. The experiments meet these conditions so that (A 1) is applicable. Equation (A 1) includes cubic nonlinearity which is the leading-order nonlinearity in some neighbourhood of the turning point where the coefficient of the quadratic nonlinearity (A 3) is zero. The dissipation is given by the integral on the right-hand side of (A 1) and the dissipation coefficient (A 6) includes the effects of laminar bottom, sidewall and interfacial boundary layers. The KdV equation assumes undirectional propagation and does not account for reflection. Since the theory is for weakly nonlinear waves it cannot predict wave breaking. However, it should give good estimates of dissipation up to the neighbourhood of the break point.

To obtain an estimate of the dissipation of a solitary wave from the beginning of the slope up to the break point, (A 1) was integrated numerically (Helfrich *et al.* 1984). The initial condition was a solitary wave of amplitude $a_0 = -0.9$, -1.9, -2.6 or -3.3 cm at the beginning of the slope. The parameters were set to the experimental conditions: $(d_+, w, \Delta\rho/\rho, \nu) = (10\text{ cm},\ 40\text{ cm},\ 0.024,\ 0.01\text{ cm}^2\text{ s}^{-1})$, $d_- = 26$ cm at the beginning of the slope, and $s = 0.034$, 0.050 or 0.067. The integration was continued up to the break point given from figure 6 for each value of λ. The incident energy E_0 was evaluated using the initial condition and the numerical solution for $\eta(t)$ at the break point was used in (13) to compute E_{BP}.

Appendix B

Consider a tank of length X_{TP} initially filled with two layers, each of depth d, with densities ρ_0 and $\rho_0+\epsilon$. Energy is put into the tank at one end creating a volume of mixed fluid with density $\rho_0+\frac{1}{2}\epsilon$. A vertical gate is placed in the tank which contains the mixed fluid in a region X_{BP} long. The thickness of the mixed fluid behind the gate is 2μ. The potential energy change in the system is found from (14), with $B(z) = X_{\mathrm{BP}}$, to be

$$\Delta P_{\mathrm{BP}} = X_{\mathrm{BP}} \tfrac{1}{4} g \epsilon \mu^2. \tag{B 1}$$

The gate is then removed and the mixed fluid is allowed to spread the length of the tank. The new thickness of the mixed fluid 2δ is

$$2\delta = (X_{\mathrm{BP}}/X_{\mathrm{TP}})\, 2\mu. \tag{B 2}$$

The increase of the potential energy of the system without the gate from the potential energy of the system before mixing, ΔP_{TP}, is

$$\Delta P_{\mathrm{TP}} = X_{\mathrm{TP}} \tfrac{1}{4} g \epsilon \delta^2 = (X_{\mathrm{BP}}^2/X_{\mathrm{TP}}) \tfrac{1}{4} g \epsilon \mu^2, \tag{B 3}$$

where (B 2) has been used. Thus, from (B 1) and (B 3),

$$\Delta P_{\mathrm{BP}} = \Delta P_{\mathrm{TP}} X_{\mathrm{TP}}/X_{\mathrm{BP}}. \tag{B 4}$$

This analysis can be generalized to N layers produced by mixing with the result given by (B 4).

REFERENCES

BENJAMIN, T. B. 1967 Internal waves of permanent form in fluids of great depth. *J. Fluid Mech.* **29**, 559–592.

CACCHIONE, D. A. & SOUTHARD, J. B. 1974 Incipient sediment movement by shoaling internal gravity waves. *J. Geophys. Res.* **79**, 2237–2242.

CACCHIONE, D. A. & WUNSCH, C. 1974 Experimental study of internal waves over a slope. *J. Fluid Mech.* **66**, 223–239.

CHAPMAN, D. C., GEISE, G. S., COLLINS, M. G., ENCARNACION, R. & JACINTO, G. 1991 Evidence of internal swash associated with Sulu Sea Solitary waves? *Cont. Shelf Res.* **11**, 591–599.

DAVIS, R. E. & ACRIVOS, A. 1967 Solitary internal waves in deep water. *J. Fluid Mech.* **29**, 593–607.

DJORDJEVIC, V. D. & REDEKOPP, L. G. 1978 The fission and disintegration of internal solitary waves moving over two-dimensional topography. *J. Phys. Oceanogr.* **8**, 1016–1024.

FU, L. L. & HOLT, B. 1982 Seasat views oceans and sea ice with synthetic aperture radar. *JPL Publications*, pp. 81–120, Feb. 15.

HAURY, L. R., BRISCOE, M. G. & ORR, M. H. 1978 Tidally generated internal wave packets in the Massachusetts Bay. *Nature* **278**, 312–317.

HELFRICH, K. R. & MELVILLE, W. K. 1986 On long nonlinear internal waves over slope–shelf topography. *J. Fluid Mech.* **167**, 285–308 (referred to herein as HM).

HELFRICH, K. R., MELVILLE, W. K. & MILES, J. W. 1984 On interfacial solitary waves over slowly varying topography. *J. Fluid Mech.* **149**, 305–317.

IVEY, G. N. & IMBERGER, J. 1991 On the nature of turbulence in a stratified fluid. Part 1. The energetics of mixing. *J. Phys. Oceanogr.* **21**, 650–658.

IVEY, G. N. & NOKES, R. I. 1989 Vertical mixing due to the breaking of critical internal waves on sloping boundaries. *J. Fluid Mech.* **204**, 479–500.

KAO, T. W., PAN, F.-S. & RENOUARD, D. 1985 Internal solitons on the pycnocline: generation, propagation, and shoaling and breaking over a slope. *J. Fluid Mech.* **169**, 19–53.

KNICKERBOCKER, C. J. & NEWELL, A. C. 1980 Internal solitary waves near a turning point. *Phys. Lett.* **75A**, 326–330.

OSBORNE, A. R. & BURCH, T. L. 1980 Internal solitons in the Andaman Sea. *Science* **208**, 451–459.

PHILIPS, O. M. 1970 On flows induced by diffusion in a stably stratified fluid. *Deep Sea Res.* **17**, 435–443.

SANDSTROM, H. & ELLIOTT, J. A. 1984 Internal tide and solitons on the Scotian Shelf: a nutrient pump at work. *J. Geophys. Res.* **89**, 6415–6426.

SEGUR, H. & HAMMACK, J. L. 1982 Soliton models of long internal waves. *J. Fluid Mech.* **118**, 285–304.

WALLACE, B. C. & WILKINSON, D. L. 1988 Run-up of internal waves on a gentle slope in a two-layered system. *J. Fluid Mech.* **191**, 419–442 (referred to herein as WW).

WHITHAM, G. B. 1974 *Linear and Nonlinear Waves*. Wiley.